Atomic-Scale Identification of Individual Lanthanide Dopants in Optical Glass Fiber

Teruyasu Mizoguchi,[†,*] Scott D. Findlay,[‡] Atsunobu Masuno,[†] Yoshihiro Saito,[§] Koji Yamaguchi,[⊥] Hiroyuki Inoue,[†] and Yuichi Ikuhara[∥]

[†]Institute of Industrial Science, University of Tokyo, 153-8505, Tokyo, Japan, [‡]School of Physics, Monash University, Victoria 3800, Australia, [§]Sumitomo Electric Industries, Ltd., Yokohama, 244-8588, Japan, [⊥]Sumitomo Electric Industries, Ltd., Osaka, 554-0024, Japan, and [∥]Institute of Engineering Innovation, University of Tokyo, 113-8505, Tokyo, Japan. T.M. performed STEM observations and wrote the manuscript. MD simulation and STEM image simulation were performed by H.I., S.D.F., and Y.I. A.M., Y.S., and K.Y. fabricated the specimen.

ABSTRACT Various dopants are added in commercially available optical glass fibers. The specific atomic species and charge state of lanthanide dopants are known to significantly influence the fiber's optical properties. For understanding the role of dopants on the optical properties, atomic-scale identification of the lanthanide dopants in the optical fiber is crucial. Aberration-corrected scanning transmission electron microscopy (STEM) is especially powerful for visualizing individual atoms of heavy elements buried in a matrix composed of light elements. Here, we apply aberration-corrected high-angle annular dark field (HAADF)-STEM to directly visualize individual erbium (Er) dopants buried in the optical glass fiber. Molecular dynamics and image simulations are used to interpret the experimental images and draw quantitative conclusions. The visibility of the buried Er atoms in the amorphous glass is strongly dependent on the defocus and specimen thickness, and only Er atoms in very thin regions can be reliably identified.

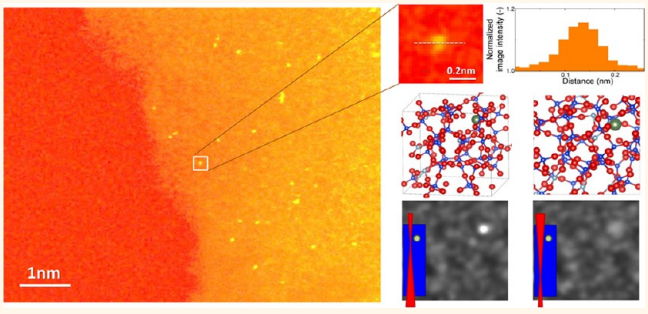

KEYWORDS: optical glass fiber · dopant · amorphous · atomic resolution STEM

Disparate areas and countries divided by great distances across the globe are, in this Internet age, linked with each other by newly developed communication tools. Internet communication is accomplished *via* a worldwide optical fiber communications network. The most important optical component for realizing intercontinental long-distance communication has been optical fiber amplifiers, which can amplify optical signals to compensate for the natural decrease in signal intensity during long-distance transfer. These amplifiers are generally made from Er^{3+}-doped silica glass and take advantage of the fluorescence of Er^{3+} when excited by a semiconductor laser. Erbium-doped fiber amplifiers (EDFA) are an indispensable element of photonics networks today.

For future high-capacity transmission systems, direct and simultaneous amplification of multiple signals is required. Over the years, various factors for improving the optical characteristics of EDFA have been investigated. It is well known that intensity of the fluorescence increases with an increase of Er^{3+} concentration, but only up to a particular concentration, usually 100 ppm or less, beyond which it saturates. This behavior is explained by concentration quenching due to the aggregation of Er^{3+} ions. Co-doping Al^{3+}, Ge^{4+}, or P^{5+} with Er^{3+} has proven useful for improving the performance of EDFA.[1−3] This is believed to be because the co-dopants surround and enclose each Er^{3+} ion, thus preventing Er^{3+} ion aggregation. Some studies have been performed to capture evidence of the local structure around Er^{3+} ions. However, spectroscopic methods, such as extended X-ray absorption fine structures (EXAFS),[2,4−6] have as yet failed to show us the atomic environment around single Er^{3+} ions because the information obtained through these methods is essentially averaged across multiple Er^{3+} ions. To find an efficient way to control the

* Address correspondence to teru@iis.u-tokyo.ac.jp.

Received for review February 5, 2013 and accepted May 22, 2013.

Published online May 28, 2013
10.1021/nn400605z

distribution of Er atoms in glass fibers and to improve the optical performance, direct and spatially resolved observation of Er atoms, which has not hitherto been achieved, is vital.

Recent developments in high-resolution transmission electron microscopy can provide us with images of single atoms and their chemical information. In particular, in aberration-corrected scanning transmission electron microscopy (STEM) an annular-type detector can be used to collect electrons scattered through high angles.[7] For a large detector inner radius, the image intensity is approximately proportional to the square of the atomic number (Z). The strong atomic number dependence of HAADF-STEM imaging is ideal for visualizing heavy elements buried in materials composed of relatively light elements. The direct observation of heavy elements inside amorphous materials using HAADF-STEM has been applied to lanthanide dopants inside grain boundary glassy films in crystalline Si_3N_4.[8−10] The method was also applied to hafnium atoms inside gate amorphous oxides formed on crystalline Si substrate.[11] However, to the best of the authors' knowledge, there are no reports on the direct observation of heavy elements inside bulk glasses. In this study, we apply atomic resolution HAADF-STEM to directly visualize the distribution of Er atoms in optical glass fibers. We believe that HAADF-STEM imaging is, at present, the only way to verify directly the Er^{3+} dispersion resulting from co-doping. For further quantitative interpretation of the information in the experimental images, molecular dynamics and image simulations are used.

RESULTS AND DISCUSSION

Figure 1 shows simultaneously acquired HAADF and BF images of an Er-doped glass fiber. Random phase contrast is evident in the BF image, but no lattice fringes, indicating that the glass fiber is amorphous and does not have any long-range ordered structure. However, bright spots are clearly visible in the HAADF image. As a particular example, the spot enclosed by the square in Figure 1a is approximately 18% brighter than the immediately surrounding glass area (Figure 1b,c). On simple Z^2 scaling, we might expect that Er (Z = 68) should be much brighter than this. However, as discussed later, the visibility of the Er buried in the glass is strongly dependent on the thickness and the position of the electron beam waist. Moreover, the height of the peak above the background is also sensitive to incoherent effects such as finite effective source size. Nevertheless, the qualitative conclusion that a bright spot indicates the presence of some heavier elements than those of silica in the glass fiber is sound. Furthermore, no such bright spots were observed in a nondoped glass fiber (see Supporting Information Figure S1). Although energy dispersive X-ray spectroscopy (EDS) and electron energy loss spectroscopy (EELS) cannot detect the Er dopants due to their low concentration, approximately 0.08 atomic %, the specimen preparation procedure and the separately performed EPMA analysis confirm that the only heavier element present is Er. The lateral scale and low Er concentration strongly suggest that the bright spots are individual Er atoms.

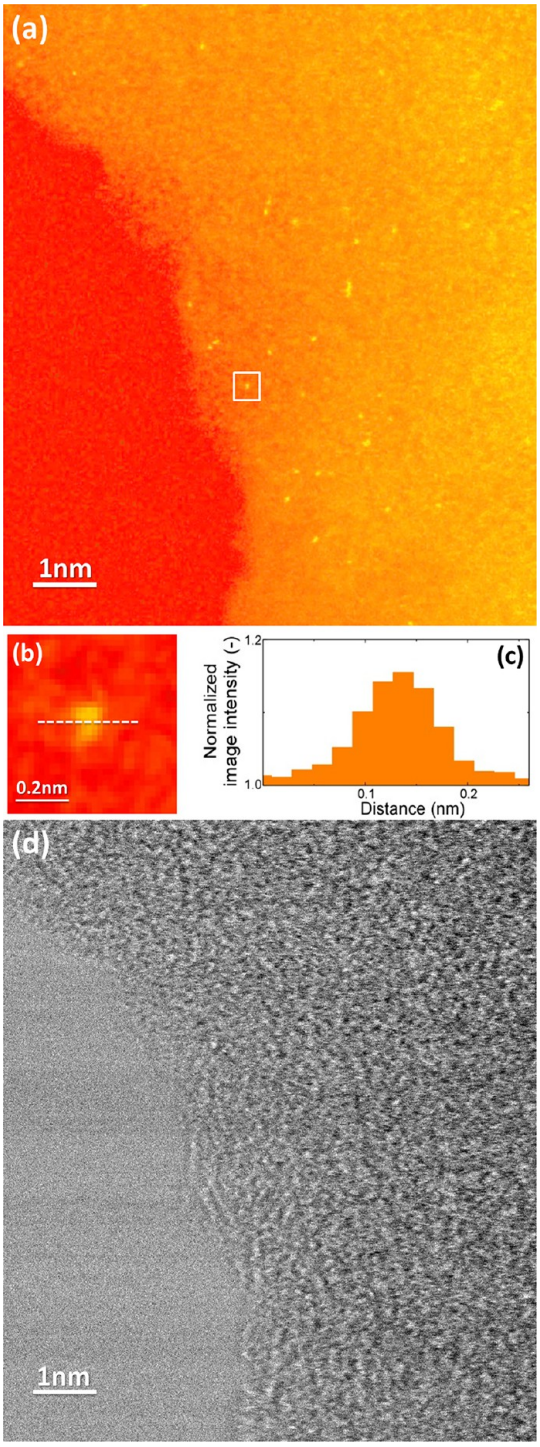

Figure 1. (a) HAADF and (d) BF-STEM images of an Er-doped glass fiber. (b) Magnified image from the rectangle area in (a). (c) Line profile of the image intensity along the dashed line in (b). The sampling interval, 0.02 nm, corresponds to the step size in the raster scan of the probe.

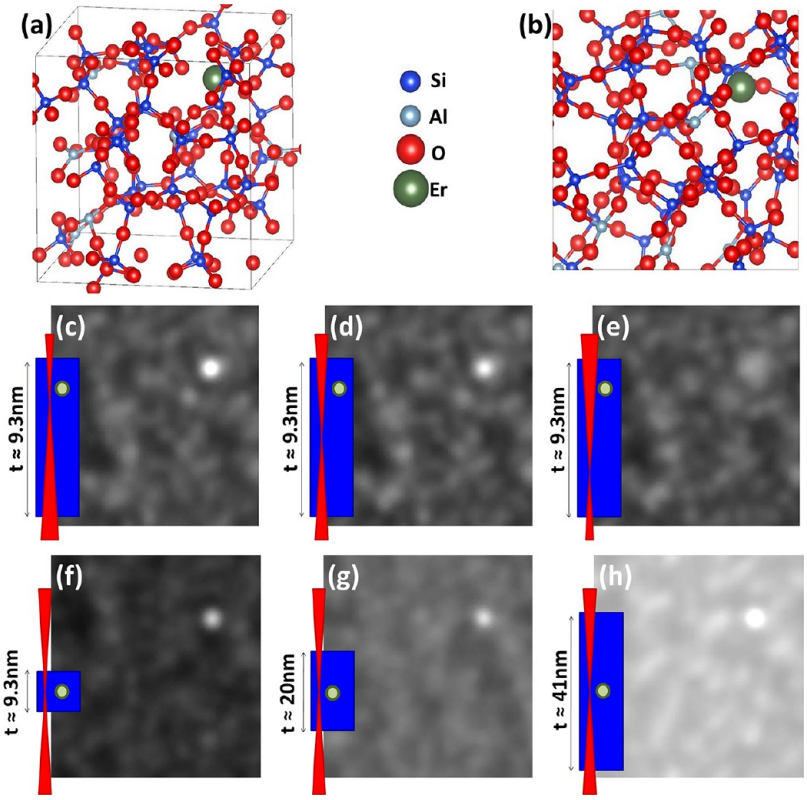

Figure 2. (a, b) Atomic coordination around an Er dopant simulated by molecular dynamics. Simulated HAADF images with 9.3 nm specimen thickness for the defocus conditions (c) 2 nm, (d) 4.7 nm, and (e) 7.3 nm. Simulated HAADF images focused on Er position for the specimen thicknesses (f) 9.3 nm, (g) 20 nm, and (h) 41 nm. The beam waist and dopant Er atom were both positioned at the midplane in (f)−(h).

However, the following two puzzling points arise from the experimental image. First, the bright spots mainly appear in the thinner area (left side of the image), being less abundant in the thicker area (right-hand side of the image). This seemingly contradicts the assumption that Er atoms are uniformly distributed in the specimen. Second, the number of the bright spots is smaller than that estimated from the specimen thickness, which we will obtain from analysis presently, and the assumption of a uniform Er distribution. Approximately 140 bright spots should appear in the area of Figure 1, assuming a mean thickness of 13 nm, whereas fewer than 50 bright spots can be identified. Put another way, the Er concentration estimated by visual analysis of the HAADF-STEM image is approximately one-third of the nominal concentration. This discrepancy implies that the HAADF-STEM image is not showing all dopant Er atoms present in the full material volume. To resolve these issues, we turn to HAADF-STEM image simulation.

To perform a meaningful HAADF-STEM image simulation, a realistic model structure is required. To construct such a model for an Er-doped glass fiber, classical molecular dynamics (MD) calculations were performed. Figure 2a and b show the simulated atomic structure around a single Er atom. Using the optimized atomic coordinates from the MD calculations, multislice STEM image simulations were performed using the absorptive model and an effective scattering potential.

First, the dependence on the focus depth was checked. The depth of focus under the imaging conditions used was about 7 nm, and we may anticipate variation in behavior depending on how this quantity compares with the specimen thickness. When the dopant depth differs by ~5 nm from that of the beam waist, the Er atom is hard to visually identify. Figures 2c−e assume a 9.3 nm thick specimen with a single Er dopant at a depth of 1.7 nm for defocus values 2, 4.7, and 7.3 nm. (Defocus $\Delta f = 0$ nm corresponds to the beam waist positioned on the entrance surface, with underfocus, *i.e.*, defocusing the beam into the specimen, being positive.) The $\Delta f = 2$ nm case has the beam waist at essentially the same depth as the dopant, which is clearly visible in the simulated image (Figure 2c). However, by $\Delta f = 7.3$ nm, the dopant is no longer distinguishable from intensity fluctuations in the signal from the supporting silica, consistent with the depth of focus reasoning. As expected, the signal from the amorphous silica matrix is largely insensitive to defocus.

The depth of focus effect alone would not preclude visualizing dopants in thicker regions, provided their depth falls within ~5 nm of the beam waist. However, the out-of-focus portions of the silica also contribute to the total HAADF signal. The signal from the Er dopants

thus decreases relative to the background, *i.e.*, to the intensity from the silica support, as the specimen gets thicker. There must therefore be a specimen thickness at which the "peak intensity" due to an in-focus Er dopant becomes comparable to the natural fluctuation in signal from the amorphous silica and the dopant ceases to be distinguishable. This is explored in Figure 2f–h, which assume the beam waist and a single Er dopant are both located at the specimen midplane for three increasingly thick specimens. By 40 nm, Figure 2h, the signal from the dopant is not much larger than the fluctuations in the signal from the amorphous silica. Thus only Er atoms within ~5 nm of the focus position and in a thin area (t < 50 nm, say) can be visualized in the HAADF-STEM image.

In order to apply the insights garnered from simulations to the experimental data, the specimen thickness must be determined. However, thickness is notoriously difficult to measure in transmission electron microscopy, especially from amorphous specimens. One solution lies in the recently developed technique of recording HAADF-STEM images on an absolute scale for direct, quantitative comparison with simulations. The microscope on which the present data were collected has not yet been calibrated to allow this, but this can be overcome by the following approach. We associate a signal with the Er dopant in the following way, shown schematically in Figure 3. First, a certain size of box, in this the case 16 × 16 pixels (which corresponds to 0.31 nm × 0.31 nm), the yellow box in Figure 3a, is centered on an Er atom, and the signal from all pixels inside the box is integrated. Next, the same size box is put over an area near the Er atom, as per the blue box in Figure 3a, and the signal from all pixels inside this box is integrated. This second box should not include the Er atom, but should be close enough to it that it corresponds to the same specimen thickness as that containing the Er atom. The integrated value of the blue box is hereafter called "γ". The signal contribution from the Er atom, hereafter called "β", is taken to be the difference between the integrated value of the yellow box and that of the blue box.

The results of applying this analysis to simulated data are shown in Figure 3b, which plots β against γ for a range of different thicknesses and relative dopant/beam waist depths. Assuming that the glass area is uniform, the integrated HAADF signal of the glass area, *i.e.*, γ, is essentially proportional to specimen thickness. The average value of β is largely independent of thickness; for all Er atoms we can reliably identify, the signal above background is of comparable value, justifying our interpretation of β as the signal due to the Er atom. Error bars have been estimated from the variation in the value of γ, due to the fluctuations in the HAADF signal depending on the position chosen for the reference blue box. No error has been assigned to the yellow box, since we only have one model structure

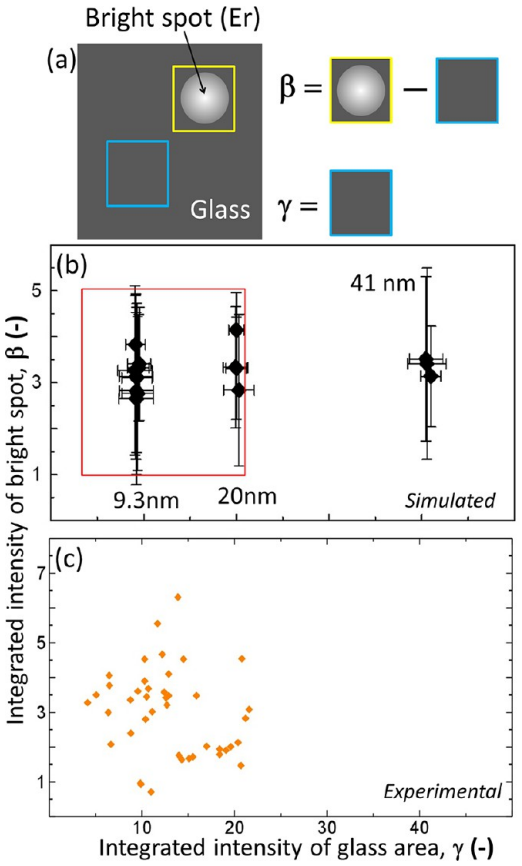

Figure 3. (a) Schematic of the present analysis. β and γ are related to the brightness of a single Er atom and the thickness, respectively. (b) Simulated and (c) experimental β–γ plots.

for simulation. It is important to appreciate therefore that the error in β is identical to the error in γ. The errors are thus correlated, with the minimum value of β occurring when the maximum value of γ is used. Though the error bars on β are quite large, as is to be expected for a small signal on top of a much larger background, β nevertheless remains strictly positive within error bars, meaning that in all the data points deemed visible and thus included in this plot, the Er signal is reliably identified above the background. This interpretation is further supported by visual inspection: the excess signal in the yellow box is attributed to the highly localized peak expected for the HAADF signal from a single dopant atom (rather than, say, a large but delocalized signal in the background contribution from the supporting glass fiber).

This analysis was applied to the HAADF image of Figure 1, which includes 42 reliably identifiable bright spots. The elongated bright spots, which may originate from the presence of Er atoms that, at least in projection, are in close lateral proximity, were eliminated from the present analysis. In simulation, we found β to be essentially independent of the specimen thickness. We therefore rescale the experimental data such that the mean value of β agrees with that in our simulations. This follows because it has been established that our simulations allow for a high fidelity of quantitative

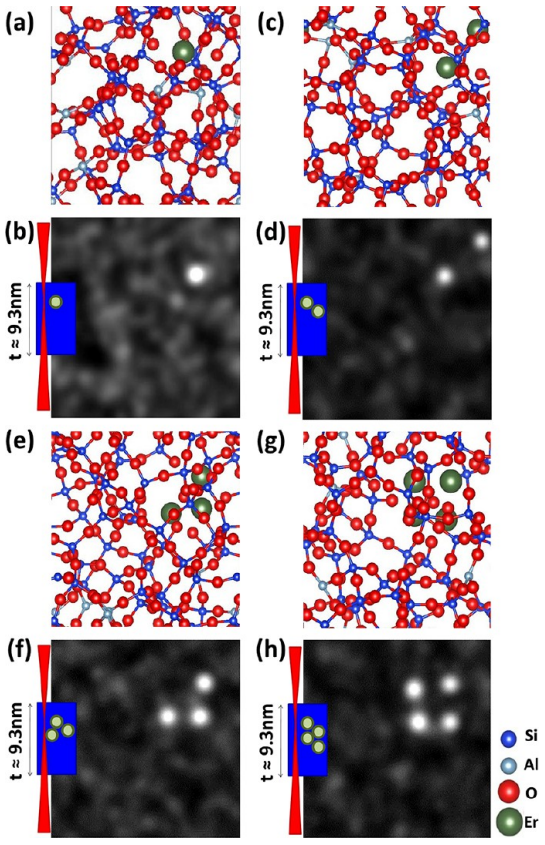

Figure 4. (a, c, e, and g) Atomic coordination around Er dopant simulated by molecular dynamic simulation, for one, two, three, and four Er atom aggregation models. (b, d, f, and h) Simulated HAADF images of the respective models. Thickness and defocus were set to 9.3 and 2 nm, respectively, and the position of the beam waist corresponds to that of the Er cluster.

comparison,[12] even though, in this experiment, the quantification was not achieved experimentally. That this scaling shows the fluctuation in β values for both the experimental and simulated data to be comparable further validates this approach. The β and γ values are, by construction, on the same scale and so are scaled the same way. It is thus found that all experimental bright spots are obtained from an area thinner than 40 nm (Figure 3c). We can now explain the puzzling points mentioned previously: only Er atoms present in thin areas (thinner than 50 nm) and close to the beam waist (closer than 5 nm) can be visualized by the present method.

A comment is warranted on the selection of the box size. The box needs to be large enough to fully encompass the dopant (the atomic size of Er is 1.7 Å). However, the error in obtaining the fixed-magnitude signal from the Er atom by taking the difference between much larger numbers (signal to background) increases with increasing box size. We found that a box size of 16 × 16 pixels (which corresponds to 0.31 nm × 0.31 nm) provided a reasonable compromise. The dependence on the box size is explored in Figure S2 (see the Supporting Information), and it can be seen that although the spread in the data changes somewhat with box size, the interpretation and thus qualitative visibility do not.

To confirm that the observed bright spots do not come from aggregated Er atoms, similar simulations were performed for Er aggregated models. The specimen thickness and defocus were set to 9.3 and 2 nm, respectively, and the beam waist was situated near the position of the Er aggregation. The distance between Er atoms in the aggregated models was 0.33−0.36 nm. These simulations are shown in Figure 4. It is clearly seen that the individual Er atoms within the Er clusters are resolved. The atoms would have to be much closer to each other than the present Er−Er distance for the peaks to merge into a single bright spot. However, closer Er−Er distances are unstable: the Er−Er distance in a stable Er oxide, Er_2O_3, is approximately 0.35 nm. This result also supports the deduction that the observed bright spots shown in Figure 1 are isolated Er atoms buried in the optical glass fiber.

CONCLUSION

In summary, we have achieved direct observation of individual Er atoms in an optical glass fiber using aberration-corrected HAADF-STEM. Molecular dynamics simulations and multislice image simulations were used to interpret the experimental images and draw quantitative conclusions. We revealed that the visibility of Er atoms in amorphous glass fiber is strongly dependent on the defocus and specimen thickness. Er atoms that are placed in the thin area, thinner than 50 nm, and are close to the beam waist, closer than 5 nm, can be identified by the present method.

This study shows that the best way to improve the visibility of the heavy elements buried in an amorphous structure is to make the specimen as thin as possible and endeavor to select a defocus value such that the beam waist is centered on the depth of the heavy element of interest. Furthermore, aberration-correction permitting, using a wider probe-forming aperture would improve the localization of the electron probe and so help maximize the signal from the dopant heavy elements.

The present approach can achieve atomic-scale determination of the distribution of heavy elements buried in amorphous optical glass. This has potential to provide further comprehensive understanding of the dopant effects on the optical properties.

METHOD

Fabricating Optical Glass. Er-doped optical fiber preforms were prepared by the modified chemical vapor deposition (MCVD) method and then drawn into fibers using silica-based fiber fabrication. Er_2O_3 of 2000 weight ppm (approximately 0.08 atomic ppm) was doped in silicate fiber, and 5.6 mol % Al_2O_3

TABLE 1. Parameters for MD Simulation

element		Z
Si		2.40
Al		1.95
Er		2.10
O		−1.21
bond	***B* (J)**	**ρ (Å)**
Si−O	2.14×10^{-15}	0.174
Al−O	3.51×10^{-16}	0.235
Er−O	4.27×10^{-16}	0.280
O−O	6.25×10^{-17}	0.362

was also doped to control the Er distribution. The constituent elements are thus Si, O, Al, and Er. The dopant concentration of each sample was confirmed by an electron probe microanalyzer (EPMA). The concentration of Er was double-checked from the optical absorption at a wavelength of around 1.53 μm. Note that the atomic weight of Er is much larger than other elements in the present system.

Scanning Transmission Electron Microscopy Observation. For STEM observation, the cladding portion of the fibers was removed by mechanical cutting and gliding, and the core of the fibers was ground into powder. Specimens for STEM observation were prepared by dropping the powder onto perforated amorphous carbon films supported on Cu grids. No heating or Ar-sputtering was applied in our specimen preparation. HAADF-STEM observations were performed using a JEOL ARM-200CF equipped with a spherical aberration corrector (CEOS Gmbh) and cold field emission gun. The probe-forming aperture angle was 24.5 mrad, while the HAADF and bright field (BF) detectors spanned the ranges 68−280 and 0−17 mrad, respectively. The spatial resolution of the present observation is approximately 0.1 nm.

Molecular Dynamics Simulation. In the molecular dynamics simulation, structural models with 3000 atoms were prepared so as to reproduce the fluorescence at 1.5 μm. The Born−Mayer type of pair potentials used are given by

$$\Phi_{ij}(r_{ij}) = \frac{e^2}{4\pi\varepsilon_0}\frac{Z_i Z_j}{r_{ij}} + B_{ij}\exp\left(-\frac{r_{ij}}{\rho_{ij}}\right) \quad (1)$$

where Φ_{ij}, the interaction energy of the ith and jth ions, consists of Coulomb and short-range repulsion terms, e is the electron charge, ε_0 is the vacuum permittivity, Z_i is the effective charge of the ith ion, r_{ij} is the interatomic distance, B_{ij} is an empirical constant, and ρ_{ij} is the softness parameter. The value of B_{ij} is obtained from the distance between i and j ions, R_{ij}, the charges of i and j ions, Z_i, Z_j, and ρ using the following equation.

$$B_{ij} = -\frac{e^2}{4\pi\varepsilon_0}\frac{Z_i Z_j}{{R_{ij}}^2}\rho\exp\left(\frac{R_{ij}}{\rho}\right) \quad (2)$$

We set the parameters for Z, B, and ρ for each atomic pair. For each cation−cation pair, the value of B was fixed at zero. The Coulomb force was evaluated using the Ewald summation. The classical equations of motion were integrated using Verlet's algorithm. All simulations were carried out at constant volume at a time step of 1 fs. The MD code for the simulations was developed by us. The potential parameters obtained by the above method are listed in Table 1.

The number of atoms was reduced to 155, including 45 Si, 7 Al, 1 Er, and 102 O atoms. Then the MD simulation was carried out again.

Multislice Image Simulation. In the STEM-image simulation, the measured experimental microscope parameters were used in calculations based on an absorptive model and using an effective scattering potential for the HAADF signal. Defocus and specimen thickness, which were not readily determinable from the experimental characterization, were varied as part of exploring the imaging dynamics. Spatial incoherence, *i.e.*, finite effective source size, was modeled as a Gaussian distribution with a half-width at half-maximum of 0.4 Å.

Conflict of Interest: The authors declare no competing financial interest.

Acknowledgment. This work is supported by MEXT (Nos. 19053001, 22686059, 23656395). STEM observation was conducted at the Research Hub for Advanced Nano Characterization, University of Tokyo, supported by MEXT. Some simulations were performed by the supercomputing system at the Institute of Solid State Physics (ISSP), University of Tokyo. This research was supported under the Discovery Projects funding scheme of the Australian Research Council (Project No. DP110101570).

Supporting Information Available: (Figure S1) HAADF and BF-STEM images of nondoped glass. (Figure S2) Box size dependence of the $\beta-\gamma$ plots. This material is available free of charge *via* the Internet at http://pubs.acs.org.

REFERENCES AND NOTES

1. Arai, K.; Namikawa, H.; Kumata, K.; Honda, T.; Ishii, Y.; Handa, T. Aluminum or Phosphorus Co-doping Effects on the Fluorescence and Structural-Properties of Neodymium-Doped Silica Glass. *J. Appl. Phys.* **1986**, *59*, 3430–3436.
2. Haruna, T.; Iihara, J.; Yamaguchi, K.; Saito, Y.; Ishikawa, S.; Onishi, M.; Murata, T. Local Structure Analyses around Er^{3+} in Er-Doped Fiber with Al Co-doping. *Opt. Express* **2006**, *14*, 11036–11042.
3. Saitoh, A.; Matsuishi, S.; Choi, S. W.; Nishii, J.; Oto, M.; Hirano, M.; Hosono, H. Elucidation of Codoping Effects on the Solubility Enhancement of Er^{3+} in SiO_2 Glass: Striking Difference between Al and P Codoping. *J. Phys. Chem. B* **2006**, *110*, 7617–7620.
4. Antonio, M. R.; Soderholm, L.; Ellison, A. J. G. Local Environments of Erbium and Lutetium in Sodium Silicate Glasses. *J. Alloys Compd.* **1997**, *250*, 536–540.
5. Bowron, D. T.; Saunders, G. A.; Newport, R. J.; Rainford, B. D.; Senin, H. B. EXAFS Studies of Rare-Earth Metaphosphate Glasses. *Phys. Rev. B* **1996**, *53*, 5268–5275.
6. Peters, P. M.; Houde-Walter, S. N. Local Structure of Er^{3+} in Multicomponent Glasses. *J. Non-Cryst. Solids* **1998**, *239*, 162–169.
7. Pennycook, S. J.; Boatner, L. A. Chemically Sensitive Structure-Imaging with a Scanning-Transmission Electron-Microscope. *Nature* **1988**, *336*, 565–567.
8. Shibata, N.; Pennycook, S. J.; Gosnell, T. R.; Painter, G. S.; Shelton, W. A.; Becher, P. F. Observation of Rare-Earth Segregation in Silicon Nitride Ceramics at Subnanometre Dimensions. *Nature* **2004**, *428*, 730–733.
9. Winkelman, G. B.; Dwyer, C.; Hudson, T. S.; Nguyen-Manh, D.; Doblinger, M.; Satet, R. L.; Hoffmann, M. J.; Cockayne, D. J. H. Three-Dimensional Organization of Rare-Earth Atoms at Grain Boundaries in Silicon Nitride. *Appl. Phys. Lett.* **2005**, 87.
10. Ziegler, A.; Idrobo, J. C.; Cinibulk, M. K.; Kisielowski, C.; Browning, N. D.; Ritchie, R. O. Interface Structure and Atomic Bonding Characteristics in Silicon Nitride Ceramics. *Science* **2004**, *306*, 1768–1770.
11. van Benthem, K.; Lupini, A. R.; Oxley, M. P.; Findlay, S. D.; Allen, L. J.; Pennycook, S. J. Three-Dimensional ADF Imaging of Individual Atoms by Through-focal Series Scanning Transmission Electron Microscopy. *Ultramicroscopy* **2006**, *106*, 1062–1068.
12. LeBeau, J. M.; Findlay, S. D.; Allen, L. J.; Stemmer, S. Quantitative Atomic Resolution Scanning Transmission Electron Microscopy. *Phys. Rev. Lett.* **2008**, 100.